

# Effect of Magnetic Field on Goos-Hänchen Shifts in Gaped Graphene Triangular Barrier

Miloud Mekkaoui<sup>a</sup>, Ahmed Jellal<sup>\*a,b</sup> and Hocine Bahlouli<sup>b,c</sup>

<sup>a</sup>*Laboratory of Theoretical Physics, Faculty of Sciences, Chouaib Doukkali University,  
PO Box 20, 24000 El Jadida, Morocco*

<sup>b</sup>*Saudi Center for Theoretical Physics, Dhahran, Saudi Arabia*

<sup>c</sup>*Physics Department, King Fahd University of Petroleum & Minerals,  
Dhahran 31261, Saudi Arabia*

## Abstract

We study the effect of a magnetic field on Goos-Hänchen shifts in gaped graphene subjected to a double triangular barrier. Solving the wave equation separately in each region composing our system and using the required boundary conditions, we then compute explicitly the transmission probability for scattered fermions. These wavefunctions are then used to derive the Goos-Hänchen shifts in terms of different physical parameters such as energy, electrostatic potential strength and magnetic field. Our numerical results show that the Goos-Hänchen shifts are affected by the presence of the magnetic field and depend on the geometrical structure of the triangular barrier.

PACS numbers: 72.80.Vp, 73.21.-b, 71.10.Pm, 03.65.Pm

Keywords: graphene, triangular double barrier, scattering, Goos-Hänchen shifts.

---

\*a.jellal@ucd.ac.ma

# 1 Introduction

Quantum and classical analogies between phenomena occurring in two different physical systems can be at the origin of discovering new effects that are relevant in device applications, and often help to understand both systems better [1]. It is well known that a light beam totally reflected from an interface between two dielectric media undergoes lateral shift from the position predicted by geometrical optics [2]. The close relationship between optics and electronic results from the fact that the electrons behave as de Broglie wave due to the ballistic transport properties of a highly mobility two-dimensional electron gas created in semiconductor heterostructures [3]. The recent discovery of graphene [4,5] added a new twist to this well established optical analogy of ballistic electron transport.

Graphene remains among the most fascinating and attractive subject in condensed matter physics. This is because of its exotic physical properties and the apparent similarity of its mathematical model to the one describing relativistic fermions in two-dimensions. As a consequence of this relativistic-like behavior particle could tunnel through very high barriers in contrast to the conventional tunneling of non-relativistic particles, an effect known in relativistic field theory as Klein Tunneling. This tunneling effect has already been observed experimentally [6] in graphene systems. There are various ways for creating barrier structures in graphene [7,8], for instance it can be done by applying a gate voltage, cutting the graphene sheet into finite width to create nanoribbons, using doping or through the creation of a magnetic barrier. In the case of graphene, computation of the transmission coefficient and the tunneling conductance were already reported for electrostatic barriers [8–11], magnetic barriers [10,12,13], potential barrier [14] and triangular barrier [16].

During the past few years there was a progress in studying the optical properties in graphene systems such as the quantum version of the Goos-Hänchen (GH) effect originating from the reflection of particles from interfaces. The GH effect was discovered by Hermann Fritz Gustav Goos and Hilda Hänchen [2] and theoretically explained by Artman [17] in the late of 1940s. Many works in various graphene-based nanostructures, including single [18], double barrier [19], and superlattices [20], showed that the GH shifts can be enhanced by the transmission resonances and controlled by varying the electrostatic potential and induced gap [18]. Similar to observations of GH shifts in semiconductors, the GH shifts in graphene can also be modulated by electric and magnetic barriers [21], an analogous GH like shift can also be observed in atomic optics [22]. It has been reported that the GH shift plays an important role in the group velocity of quasiparticles along interfaces of graphene p-n junctions [23,24]. Experimentally when graphene is deposited on dielectric materials it results in a profound effect on GH where it can be either positive or negative with a complete electrostatic control [25,26]. Recently it has been shown that nonlinear surface plasmon resonance in graphene can provide rigorous enhancement and control over GH effect [27,28].

Very recently, we have studied the GH shift exhibited by Dirac fermions in graphene scattered by triangular double barrier [29]. We extend our former work [29] to include the effect of an external magnetic field on the Goos-Hänchen shifts in a gaped graphene triangular barrier. By separating our system into five regions, we determine the solutions of the energy spectrum in terms of different physical quantities in each region. After matching the wavefunctions at different interfaces of potential width, we determine the transmission probability and subsequently the GH shifts. To acquire a better understanding of our results, we plot the GH shifts for different values of the physical parameters

characterizing our system. We also show that the GH shifts can be influenced by the applied magnetic field and can be positive or negative according to the values taken by the physical parameters. In addition, interesting discussions and comments will be reported in different occasions.

The present paper is organized as follows. In section 2, we formulate our model by setting the Hamiltonian system describing particles scattered by a triangular double barrier whose intermediate zone is subject to a mass term. We also obtain the spinor solution corresponding to each regions composing our system in terms of different physical parameters. Using the transfer matrix resulting from the boundary conditions, we determine the corresponding transmission probability in section 3. In section 4, we derive the analytical form of the GH shifts and in section 5 we present the main numerical results for the GH shifts and transmission probability of the particle beam transmitted through graphene triangular double barrier. Finally, in section 6 we conclude our work and summarize our main findings.

## 2 Model of the system

We consider massless Dirac particles with energy  $E$  and incident angle  $\phi_1$  with respect to the incident  $x$ -direction of a gaped graphene triangular double barrier. This system is a flat sheet of graphene subject to a triangular potential barrier along the  $x$ -direction while particles are free in the  $y$ -direction. To ease our task let us first describe the geometry of our system which is made of five regions denoted by  $j = 1, \dots, 5$ . Each region is characterized by its potential and interaction with external sources. The barrier regions are formally described by the Dirac-like Hamiltonian

$$H = v_F \boldsymbol{\sigma} \cdot \left( \mathbf{p} + \frac{e}{c} \mathbf{A}(x, y) \right) + V(x) \mathbb{I}_2 + \Delta \sigma_z \quad (1)$$

where  $v_F \approx 10^6 m/s$  is the Fermi velocity,  $\boldsymbol{\sigma} = (\sigma_x, \sigma_y)$  are the Pauli matrices,  $\mathbf{p} = -i\hbar(\partial_x, \partial_y)$ ,  $\mathbb{I}_2$  the  $2 \times 2$  unit matrix. The vector potential will be chosen in the Landau gauge  $\mathbf{A}(x, y) = (0, A_y(x))$  with the magnetic field  $\partial_x A_y(x) = B(x)$ . The parameter  $\Delta = mv_F^2$  is the energy gap owing to the sublattice symmetry breaking or can be seen as originating from spin-orbit interaction  $\Delta = \Delta_{so}$ , and is confined to the region  $|x| \leq d_1$

$$\Delta = t' \Theta(d_1^2 - x^2) \quad (2)$$

where  $\Theta$  is the Heaviside step function. The double triangular barrier  $V(x)$  is described by the following potential configuration

$$V(x) = V_j = \begin{cases} (\gamma x + d_2)F, & d_1 \leq |x| \leq d_2 \\ V_2, & |x| \leq d_1 \\ 0, & \text{otherwise} \end{cases} \quad (3)$$

where  $\gamma = 1$  for  $x \in [-d_2, -d_1]$ ,  $\gamma = -1$  for  $x \in [d_1, d_2]$  and  $F = \frac{V_1}{d_2 - d_1}$ , it is presented schematically in Figure 1. We introduce a uniform perpendicular magnetic field, along the  $z$ -direction, constrained to the well region between the two barriers (Figure 1) such that

$$B(x) = B \Theta(d_1^2 - x^2) \quad (4)$$

where  $B$  is the strength of the magnetic field within the strip located in the region  $|x| > d_1$  and  $B = 0$  otherwise. We recall that experimentally, different electrostatic profiles can be imposed on the

sample using different methods such as subjecting it to electrostatic gate or changing the doping level as well as defects density. The triangular profile (Figure 1) or trapezoidal electrostatic barriers can be achieved for example by imposing an inhomogeneous doping into the sample [30]. On the other hand, the magnetic field profile imposed on the sample can be provided externally using a magnetic strip.

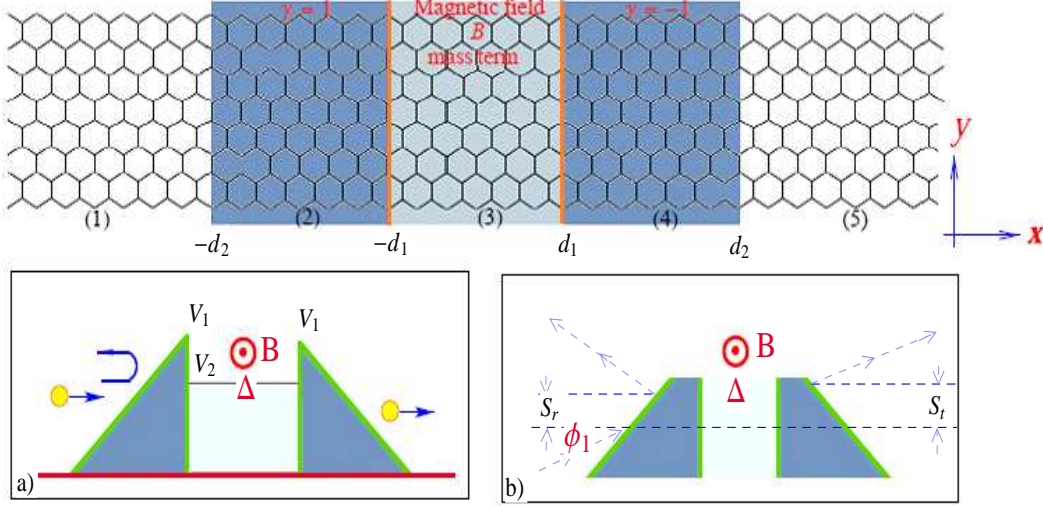


Figure 1: Schematic plots of the models that we are considering, the light shaded area in the upper subplot represents Dirac fermions in inhomogeneous magnetic field through a graphene triangular double barriers. (a): The shaded area show smooth electric potentials with error function distributions. (b): Describes the incident, reflected and transmitted electron beams with lateral shifts  $S_r$  and  $S_t$ .

Choosing the Landau gauge and imposing continuity of the vector potential at the boundaries to avoid nonphysical effects, we end up with the following vector potential

$$A_y(x) = A_j = \frac{c}{el_B^2} \times \begin{cases} -d_1, & x < -d_2 \\ x, & |x| < d_1 \\ d_1, & x \geq d_2 \end{cases} \quad (5)$$

where the magnetic length is  $l_B = \sqrt{1/B}$  in the unit system  $\hbar = c = e = 1$ . Recall that our system contains five regions denoted  $j = 1, \dots, 5$ . The left region ( $j = 1$ ) describes the incident electron beam with energy  $E = v_F \epsilon$  and incident angle  $\phi_1$  where  $v_F$  is the Fermi velocity. The right region ( $j = 5$ ) describes the transmitted electron beam with angle  $\phi_5$ . The time-independent Dirac equation for the spinor  $\psi_j(x, y) = (\varphi_j^+, \varphi_j^-)^T$  at energy  $E = v_F \epsilon$  reads as

$$\left[ \boldsymbol{\sigma} \cdot \left( \mathbf{p} + \frac{e}{c} \mathbf{A}(x, y) \right) + v_j \mathbb{I}_2 + \mu \Theta(d_1^2 - x^2) \sigma_z \right] \psi_j(x, y) = \epsilon \psi_j(x, y) \quad (6)$$

where we have defined  $V_j = v_F v_j$  and  $t' = v_F \mu$  and  $F = v_F \varrho$ . To proceed further, we need to find the solutions of the corresponding Dirac equation according to each region  $j = 1, \dots, 5$ . Indeed, for  $x < -d_2$  (region 1):

$$\epsilon = \left[ p_{x1}^2 + \left( p_y - \frac{1}{l_B^2} d_1 \right)^2 \right]^{\frac{1}{2}} \quad (7)$$

$$\psi_1(x, y) = \frac{1}{\sqrt{2}} \begin{pmatrix} 1 \\ z_1 \end{pmatrix} e^{i(p_{x1}x + p_y y)} + r \frac{1}{\sqrt{2}} \begin{pmatrix} 1 \\ -z_1^* \end{pmatrix} e^{i(-p_{x1}x + p_y y)} \quad (8)$$

$$z_1 = s_1 \frac{p_{x1} + i \left( p_y - \frac{1}{l_B^2} d_1 \right)}{\sqrt{p_{x1}^2 + \left( p_y - \frac{1}{l_B^2} d_1 \right)^2}} \quad (9)$$

For  $x > d_2$  (region 5):

$$\epsilon = \left[ p_{x5}^2 + \left( p_y + \frac{1}{l_B^2} d_1 \right)^2 \right]^{\frac{1}{2}} \quad (10)$$

$$\psi_5(x, y) = \frac{1}{\sqrt{2}} t \begin{pmatrix} 1 \\ z_5 \end{pmatrix} e^{i(p_{x5}x + p_y y)}, \quad z_5 = s_5 \frac{p_{x5} + i \left( p_y + \frac{1}{l_B^2} d_1 \right)}{\sqrt{p_{x5}^2 + \left( p_y + \frac{1}{l_B^2} d_1 \right)^2}} \quad (11)$$

As far as  $|x| < d_1$  (region 3) is concerned, we first write down the corresponding Hamiltonian in terms of annihilation and creation operators. This can be obtained from (1)

$$H = v_F \begin{pmatrix} m^+ & -i \frac{\sqrt{2}}{l_B} a^- \\ i \frac{\sqrt{2}}{l_B} a^+ & m^- \end{pmatrix} \quad (12)$$

where we have introduced the shell operators

$$a^\pm = \frac{l_B}{\sqrt{2}} \left( \mp \partial_x + k_y + \frac{x}{l_B^2} \right) \quad (13)$$

and the parameters  $m^\pm = v_2 \pm \mu$ . We show that the involved operators obey the canonical commutation relation  $[a^-, a^+] = \mathbb{I}$ . Note that, the energy gap  $t'$  behaves like a mass term in Dirac equation, which this will affect the above results and leads to interesting consequences on the transport properties of our system. We determine the eigenvalues and eigenspinors of the Hamiltonian  $H$  by considering the time independent equation for the spinor  $\psi_3(x, y) = (\psi_3^+, \psi_3^-)^T$  using the fact that the transverse momentum  $p_y$  is conserved to write  $\psi_3(x, y) = e^{ip_y y} \varphi_3(x)$  with  $\varphi_3(x) = (\varphi_3^+, \varphi_3^-)^T$ . Then the eigenvalue equation

$$H \begin{pmatrix} \varphi_3^+ \\ \varphi_3^- \end{pmatrix} = \epsilon \begin{pmatrix} \varphi_3^+ \\ \varphi_3^- \end{pmatrix} \quad (14)$$

gives the coupled equations

$$m^+ \varphi_3^+ - i \frac{\sqrt{2}}{l_B} a^- \varphi_3^- = \epsilon \varphi_3^+ \quad (15)$$

$$i \frac{\sqrt{2}}{l_B} a^+ \varphi_3^+ + m^- \varphi_3^- = \epsilon \varphi_3^-. \quad (16)$$

Injecting (16) into (15) we end up with a differential equation of second order for  $\varphi_3^+$

$$(\epsilon - m^+)(\epsilon - m^-) \varphi_3^+ = \frac{2}{l_B^2} a^- a^+ \varphi_3^+. \quad (17)$$

This is in fact an equation of the harmonic oscillator and therefore we identify  $\varphi_3^+$  with its eigenstates  $|n-1\rangle$  corresponding to the eigenvalues

$$\epsilon - v_2 = s_3 k_\eta = s_3 \frac{1}{l_B} \sqrt{(\mu l_B)^2 + 2n} \quad (18)$$

where we have set  $k_\eta = s_3(\epsilon - v_2)$ ,  $s_3 = \text{sign}(\epsilon - v_2)$  correspond to positive and negative energy solutions. The second spinor component can be derived from (16) to obtain

$$\varphi_3^- = s_3 i \sqrt{\frac{k_\eta l_B - s_3 \mu l_B}{k_\eta l_B + s_3 \mu l_B}} |n\rangle. \quad (19)$$

Introducing the parabolic cylinder functions

$$D_n(x) = 2^{-\frac{n}{2}} e^{-\frac{x^2}{4}} H_n\left(\frac{x}{\sqrt{2}}\right) \quad (20)$$

to express the solution in region 3 as

$$\psi_3(x, y) = b_1 \psi_3^+(x, y) + b_2 \psi_3^-(x, y) \quad (21)$$

with the two components

$$\psi_3^\pm(x, y) = \frac{1}{\sqrt{2}} \begin{pmatrix} \sqrt{\frac{k_\eta l_B + s_3 \mu l_B}{k_\eta l_B}} D((k_\eta l_B)^2 - (\mu l_B)^2)/2 - 1 \left( \pm \sqrt{2} \left( \frac{x}{l_B} + k_y l_B \right) \right) \\ \pm i \frac{s_3 \sqrt{2}}{\sqrt{k_\eta l_B (k_\eta l_B + s_3 \mu l_B)}} D((k_\eta l_B)^2 - (\mu l_B)^2)/2 \left( \pm \sqrt{2} \left( \frac{x}{l_B} + k_y l_B \right) \right) \end{pmatrix} e^{ik_y y} \quad (22)$$

In  $d_1 < |x| < d_2$  (regions 2 ( $\gamma = -1$ ) and 4 ( $\gamma = +1$ )): the general solution can be written in terms of the parabolic cylinder function [16, 31, 32] as

$$\chi_\gamma^+ = c_1 D_{\nu_\gamma-1}(Q_\gamma) + c_2 D_{-\nu_\gamma}(-Q_\gamma^*) \quad (23)$$

where we have set the parameters  $\nu_\gamma = \frac{i}{2\varrho} \left( k_y - \gamma \frac{d_1}{l_B^2} \right)^2$ ,  $\epsilon_0 = \epsilon - v_1$  and made the change of variable  $Q_\gamma(x) = \sqrt{\frac{2}{\varrho}} e^{i\pi/4} (\gamma \varrho x + \epsilon_0)$ ,  $c_1$  and  $c_2$  are two constants. The second component is given by

$$\begin{aligned} \chi_\gamma^- &= -c_2 \frac{1}{k_y - \gamma \frac{d_1}{l_B^2}} \left[ 2(\epsilon_0 + \gamma \varrho x) D_{-\nu_\gamma}(-Q_\gamma^*) + \sqrt{2\varrho} e^{i\pi/4} D_{-\nu_\gamma+1}(-Q_\gamma^*) \right] \\ &\quad - \frac{c_1}{k_y - \gamma \frac{d_1}{l_B^2}} \sqrt{2\varrho} e^{-i\pi/4} D_{\nu_\gamma-1}(Q_\gamma) \end{aligned} \quad (24)$$

The components of the spinor solution  $\psi_m(x, y) = \begin{pmatrix} \varphi_\gamma^+(x) \\ \varphi_\gamma^-(x) \end{pmatrix} e^{ik_y y}$  of the Dirac equation (6) in regions  $m=2$  ( $\gamma = -1$ ) and  $m=4$  ( $\gamma = +1$ ) can be obtained from (23) and (24) by setting

$$\varphi_\gamma^+(x) = \chi_\gamma^+ + i\chi_\gamma^-, \quad \varphi_\gamma^-(x) = \chi_\gamma^+ - i\chi_\gamma^- \quad (25)$$

and therefore obtain the eigenspinor

$$\psi_m(x, y) = a_{m-1} \begin{pmatrix} u_\gamma^+(x) \\ u_\gamma^-(x) \end{pmatrix} e^{ik_y y} + a_m \begin{pmatrix} v_\gamma^+(x) \\ v_\gamma^-(x) \end{pmatrix} e^{ik_y y} \quad (26)$$

where the functions  $u_\gamma^\pm(x)$  and  $v_\gamma^\pm(x)$  are given by

$$u_\gamma^\pm(x) = D_{\nu_\gamma-1}(Q_\gamma) \mp \frac{1}{k_y - \gamma \frac{d_1}{l_B^2}} \sqrt{2\varrho} e^{i\pi/4} D_{\nu_\gamma}(Q_\gamma) \quad (27)$$

$$\begin{aligned} v_\gamma^\pm(x) &= \pm \frac{1}{k_y - \gamma \frac{d_1}{l_B^2}} \sqrt{2\varrho} e^{-i\pi/4} D_{-\nu_\gamma+1}(-Q_\gamma^*) \\ &\quad \pm \frac{1}{k_y - \gamma \frac{d_1}{l_B^2}} \left( -2i\epsilon_0 \pm \left( k_y - \gamma \frac{d_1}{l_B^2} \right) - \gamma 2i\varrho x \right) D_{-\nu_\gamma}(-Q_\gamma^*). \end{aligned} \quad (28)$$

with  $a_m$  and  $a_{m-1}$  are four constants. The above established results will be used in the next section to derive the transmission and reflection amplitudes.

### 3 Transmission amplitude

The coefficients  $(a_1, a_2, a_3, a_4, b_1, b_2, r, t)$  can be determined using the boundary conditions, continuity of the eigenspinors at each interface. Based on different considerations, we study the interesting properties of our system in terms of the corresponding transmission probability. Before doing so, let us simplify our writing using the following shorthand notation

$$\vartheta_{\tau 1}^{\pm} = D_{[(k_{\eta} l_B)^2 - (\mu l_B)^2]/2-1} \left[ \pm \sqrt{2} \left( \frac{\tau d_1}{l_B} + k_y l_B \right) \right] \quad (29)$$

$$\zeta_{\tau 1}^{\pm} = D_{[(k_{\eta} l_B)^2 - (\mu l_B)^2]/2} \left[ \pm \sqrt{2} \left( \frac{\tau d_1}{l_B} + k_y l_B \right) \right] \quad (30)$$

$$f_1^{\pm} = \sqrt{\frac{k_{\eta} \pm \mu}{k_{\eta}}}, \quad f_2^{\pm} = \frac{\sqrt{2/l_B^2}}{\sqrt{k_{\eta}(k_{\eta} \pm \mu)}} \quad (31)$$

$$u_{\gamma}^{\pm}(\tau d_1) = u_{\gamma, \tau 1}^{\pm}, \quad u_{\gamma}^{\pm}(\tau d_2) = u_{\gamma, \tau 2}^{\pm} \quad (32)$$

$$v_{\gamma}^{\pm}(\tau d_1) = v_{\gamma, \tau 1}^{\pm}, \quad v_{\gamma}^{\pm}(\tau d_2) = v_{\gamma, \tau 2}^{\pm} \quad (33)$$

where  $\tau = \pm$ . Now, requiring the continuity of the spinor wavefunctions at each junction interface gives rise to a set of equations. We prefer to express these relationships in terms of  $2 \times 2$  transfer matrices between different regions,  $\mathcal{M}_{jj+1}$ . Then the full transfer matrix over the whole triangular double barrier can be written as

$$\begin{pmatrix} 1 \\ r \end{pmatrix} = \prod_{j=1}^4 \mathcal{M}_{jj+1} \begin{pmatrix} t \\ 0 \end{pmatrix} = \mathcal{M} \begin{pmatrix} t \\ 0 \end{pmatrix} \quad (34)$$

which is the product of four transfer matrices that couple the wave function in the  $j$ -th region to the wave function in the  $(j+1)$ -th region

$$\mathcal{M} = \mathcal{M}_{12} \cdot \mathcal{M}_{23} \cdot \mathcal{M}_{34} \cdot \mathcal{M}_{45} \quad (35)$$

and are given by

$$\mathcal{M} = \begin{pmatrix} \tilde{m}_{11} & \tilde{m}_{12} \\ \tilde{m}_{21} & \tilde{m}_{22} \end{pmatrix} \quad (36)$$

$$\mathcal{M}_{12} = \begin{pmatrix} e^{-ip_{x1}d_2} & e^{ip_{x1}d_2} \\ z_1 e^{-ip_{x1}d_2} & -z_1^* e^{ip_{x1}d_2} \end{pmatrix}^{-1} \begin{pmatrix} u_{1,-2}^+ & v_{1,-2}^+ \\ u_{1,-2}^- & v_{1,-2}^- \end{pmatrix} \quad (37)$$

$$\mathcal{M}_{23} = \begin{pmatrix} u_{1,-1}^+ & v_{1,-1}^+ \\ u_{1,-1}^- & v_{1,-1}^- \end{pmatrix}^{-1} \begin{pmatrix} \vartheta_1^+ & \vartheta_1^- \\ \zeta_1^+ & \zeta_1^- \end{pmatrix} \quad (38)$$

$$\mathcal{M}_{34} = \begin{pmatrix} \vartheta_{-1}^+ & \vartheta_{-1}^- \\ \zeta_{-1}^+ & \zeta_{-1}^- \end{pmatrix}^{-1} \begin{pmatrix} u_{-1,1}^+ & v_{-1,1}^+ \\ u_{-1,1}^- & v_{-1,1}^- \end{pmatrix} \quad (39)$$

$$\mathcal{M}_{45} = \begin{pmatrix} u_{-1,2}^+ & v_{-1,2}^+ \\ u_{-1,2}^- & v_{-1,2}^- \end{pmatrix}^{-1} \begin{pmatrix} e^{ip_{x5}d_2} & e^{-ip_{x5}d_2} \\ z_5 e^{ip_{x5}d_2} & -z_5^* e^{-ip_{x5}d_2} \end{pmatrix}. \quad (40)$$

Using these we obtain the transmission and reflection amplitudes

$$t = \frac{1}{\tilde{m}_{11}}, \quad r = \frac{\tilde{m}_{21}}{\tilde{m}_{11}} \quad (41)$$

and explicitly,  $t$  takes the form

$$t = \frac{e^{id_2(p_{x1}+p_{x5})} (1+z_5^2) (\vartheta_1^- \zeta_1^+ + \vartheta_1^+ \zeta_1^-)}{f_2^+ (f_1^- \mathcal{L}_1 + i f_2^- \mathcal{L}_2) + f_1^+ (f_2^- \mathcal{L}_3 + i f_1^- \mathcal{L}_4)} \mathcal{D} \quad (42)$$

where we have set

$$\mathcal{D} = \left( u_{-1,1}^- v_{-1,1}^+ - u_{-1,1}^+ v_{-1,1}^- \right) \left( u_{1,-2}^+ v_{1,-2}^- - u_{1,-2}^- v_{1,-2}^+ \right) \quad (43)$$

$$\mathcal{L}_1 = \vartheta_{-1}^- \zeta_1^+ \mathcal{F} \mathcal{G} - \vartheta_1^- \zeta_{-1}^+ \mathcal{K} \mathcal{J} \quad (44)$$

$$\mathcal{L}_2 = (\zeta_1^+ \zeta_{-1}^- - \zeta_1^- \zeta_{-1}^+) \mathcal{F} \mathcal{J} \quad (45)$$

$$\mathcal{L}_3 = \vartheta_{-1}^+ \zeta_1^- \mathcal{F} \mathcal{G} - \vartheta_1^+ \zeta_{-1}^- \mathcal{K} \mathcal{J} \quad (46)$$

$$\mathcal{L}_4 = (\vartheta_1^+ \vartheta_{-1}^- - \vartheta_1^- \vartheta_{-1}^+) \mathcal{K} \mathcal{G} \quad (47)$$

with the quantities

$$\mathcal{F} = \left[ u_{1,-1}^+ v_{1,-2}^- - u_{1,-2}^+ v_{1,-1}^- - z_1 \left( u_{1,-1}^+ v_{1,-2}^+ - u_{1,-2}^+ v_{1,-1}^+ \right) \right] \quad (48)$$

$$\mathcal{G} = \left[ u_{-1,1}^- v_{-1,2}^+ - u_{-1,2}^- v_{-1,1}^+ + z_5 \left( u_{-1,1}^- v_{-1,2}^- - u_{-1,2}^- v_{-1,1}^- \right) \right] \quad (49)$$

$$\mathcal{K} = \left[ u_{1,-1}^- v_{1,-2}^- - u_{1,-2}^- v_{1,-1}^- - z_1 \left( u_{1,-1}^- v_{1,-2}^+ - u_{1,-2}^- v_{1,-1}^+ \right) \right] \quad (50)$$

$$\mathcal{J} = \left[ u_{-1,1}^+ v_{-1,2}^- - u_{-1,2}^+ v_{-1,1}^- + z_5 \left( u_{-1,1}^+ v_{-1,2}^+ - u_{-1,2}^+ v_{-1,1}^+ \right) \right] \quad (51)$$

We can also write (41) in complex notation as

$$t = \rho_t e^{i\varphi_t}, \quad r = \rho_r e^{i\varphi_r} \quad (52)$$

where the phase of the transmitted  $\varphi_t$  and reflected  $\varphi_r$  amplitudes are given by

$$\varphi_t = \arctan \left( i \frac{t^* - t}{t^* + t} \right), \quad \varphi_r = \arctan \left( i \frac{r^* - r}{r^* + r} \right). \quad (53)$$

Actually what we exactly need are the transmission and reflection probabilities, which can be obtained by introducing the electric current density  $J$  corresponding to our system. Then from the previous Hamiltonian, we derive the incident, reflected and transmitted current

$$J_{\text{inc}} = e v_F (\psi_1^+)^\dagger \sigma_x \psi_1^+ \quad (54)$$

$$J_{\text{ref}} = e v_F (\psi_1^-)^\dagger \sigma_x \psi_1^- \quad (55)$$

$$J_{\text{tra}} = e v_F \psi_5^\dagger \sigma_x \psi_5. \quad (56)$$

These can be used to write the transmission and reflection probabilities as

$$T = \frac{p_{x5}}{p_{x1}} (\text{Im}[t]^2 + \text{Re}[t]^2), \quad R = \text{Im}[r]^2 + \text{Re}[r]^2. \quad (57)$$

These will be numerically computed by choosing different values of the parameters characterizing the present system. In fact, we will present different plots to underline and understand the basic properties of our system.



## 4 The Goos-Hänchen shifts

The Goos-Hänchen shifts in graphene can be analyzed by considering an incident, reflected and transmitted beams around some transverse wave vector  $k_y = k_{y0}$  and the angle of incidence  $\phi_1(k_{y0}) \in [0, \frac{\pi}{2}]$ , denoted by the subscript 0. These can be expressed in integral forms as

$$\Psi_i(x, y) = \int_{-\infty}^{+\infty} dk_y f(k_y - k_{y0}) e^{i(k_{x1}(k_y)x + k_y y)} \begin{pmatrix} 1 \\ e^{i\phi_1(k_y)} \end{pmatrix} \quad (58)$$

$$\Psi_r(x, y) = \int_{-\infty}^{+\infty} dk_y r(k_y) f(k_y - k_{y0}) e^{i(-k_{x1}(k_y)x + k_y y)} \begin{pmatrix} 1 \\ -e^{-i\phi_1(k_y)} \end{pmatrix} \quad (59)$$

and the reflection coefficient is  $r(k_y) = |r|e^{i\varphi_r}$ . This fact is represented by writing the  $x$ -component of wave vector,  $k_{x1}$  as well as  $\phi_1$  in terms of  $k_y$ , where each spinor plane wave is a solution of (6) and  $f(k_y - k_{y0})$  is the angular spectral distribution. We can approximate the  $k_y$ -dependent terms by a Taylor expansion around  $k_y$ , retaining only the first order term to get

$$\phi_1(k_y) \approx \phi_1(k_{y0}) + \frac{\partial \phi_1}{\partial k_y} \Big|_{k_{y0}} (k_y - k_{y0}) \quad (60)$$

$$k_{x1}(k_y) \approx k_{x1}(k_{y0}) + \frac{\partial k_{x1}}{\partial k_y} \Big|_{k_{y0}} (k_y - k_{y0}). \quad (61)$$

Finally, the transmitted beams are

$$\Psi_t(x, y) = \int_{-\infty}^{+\infty} dk_y t(k_y) f(k_y - k_{y0}) e^{i(k_{x1}(k_y)x + k_y y)} \begin{pmatrix} 1 \\ e^{i\phi_1(k_y)} \end{pmatrix} \quad (62)$$

and the transmission coefficient is  $t(k_y) = |t|e^{i\varphi_t}$ .

The stationary-phase approximation indicates that the GH shifts are equal to the negative gradient of transmission phase with respect to  $k_y$ . To calculate the GH shifts of the transmitted beam through our system, according to the stationary phase method [33], we adopt the definition [18, 34, 35]

$$S_t = -\frac{\partial \varphi_t}{\partial k_{y0}}, \quad S_r = -\frac{\partial \varphi_r}{\partial k_{y0}}. \quad (63)$$

Assuming a finite-width beam with the Gaussian shape,  $f(k_y - k_{y0}) = w_y \exp[-(w_y^2/2)(k_y - k_{y0})^2]$ , around  $k_{y0}$ , where  $w_y = w \sec \phi_1$ , and  $w$  is the half beam width at waist, we can evaluate the Gaussian integral to obtain the spatial profile of the incident beam, by expanding  $\phi_1$  and  $k_{x1}$  to first order around  $k_{y0}$  when satisfying the condition

$$\delta \phi_1 = \lambda_F / (\pi w) \ll 1 \quad (64)$$

where  $\lambda_F$  is Fermi wavelength. Comparison of the incident and transmitted beams suggests that the displacements  $\sigma_{\pm}$  of up and down spinor components are both equal to  $\partial \varphi_t / \partial k_{y0}$  and the average displacement is

$$S_t = \frac{1}{2}(\sigma^+ + \sigma^-) = -\frac{\partial \varphi_t}{\partial k_{y0}}. \quad (65)$$

It should be noted that when the above-mentioned condition is satisfied, that is, the stationary phase method is valid [18], the definition (63) can be applicable to any finite-width beam, not necessarily a Gaussian-shaped beam.

## 5 Discussion of numerical simulations

The numerical results for the GH shifts of Dirac electrons in graphene scattered by a triangular double barrier potential under a uniform vertical magnetic field are now presented. In fact, we numerically evaluate the GH shifts in transmission  $S_t$  and in reflection  $S_r$  regions, respectively, as a function of structural parameters of our system, including the energy  $\epsilon l_B$ , the  $y$ -direction wave vector  $k_y l_B$ , the energy gap  $\mu l_B$ , the barriers widths  $d_1/l_B$  and  $d_2/l_B$ , the strength of potential barriers  $v_1 l_B$  and  $v_2 l_B$ . First we present in Figures 2 and 3 the GH shifts in the transmission region a) and the corresponding transmission probabilities b) as function of the incident energy  $\epsilon l_B$ . We have chosen the parameters  $(v_1 l_B = 10, v_2 l_B = 20)$  in Figure 2 and  $(v_1 l_B = 20, v_2 l_B = 10)$  in Figure 3, with  $k_y l_B = 1$  and three different values of the barrier width  $\frac{d_1}{l_B} = 0.2$ ,  $\frac{d_1}{l_B} = 0.5$ ,  $\frac{d_1}{l_B} = 1.4$  corresponding to red, green and blue colors, respectively.

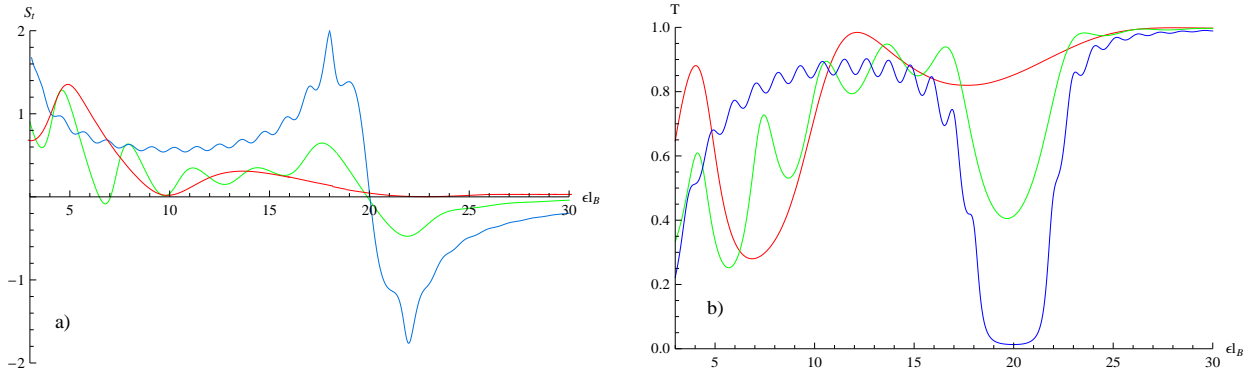


Figure 2: (Color online) a): The GH shifts in transmission  $S_t$  and b): the transmission probability  $T$  versus the incident energy  $\epsilon l_B$  with  $\frac{d_1}{l_B} = 0.2$  red color,  $\frac{d_1}{l_B} = 0.5$  green color,  $\frac{d_1}{l_B} = 1.4$  blue color,  $\frac{d_2}{l_B} = 1.5$ ,  $\mu l_B = 0$ ,  $k_y l_B = 1$  and  $(v_1 l_B = 10, v_2 l_B = 20)$ .

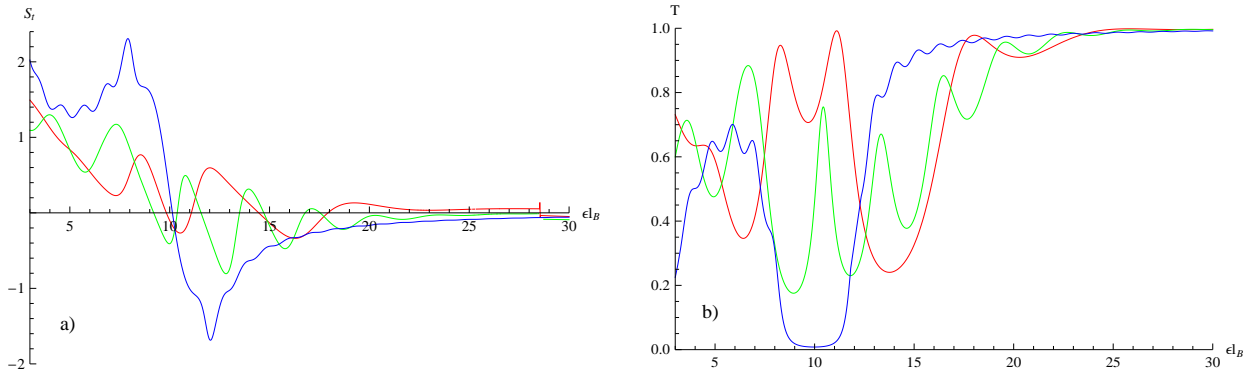


Figure 3: (Color online) a): The GH shifts in transmission  $S_t$  and b): the transmission probability  $T$  versus the incident energy  $\epsilon l_B$  with  $\frac{d_1}{l_B} = 0.2$  red color,  $\frac{d_1}{l_B} = 0.5$  green color,  $\frac{d_1}{l_B} = 1.4$  blue color,  $\frac{d_2}{l_B} = 1.5$ ,  $\mu l_B = 0$ ,  $k_y l_B = 1$  and  $(v_1 l_B = 20, v_2 l_B = 10)$ .

It is shown that the GH shifts  $S_t$  are closely related to the transmission probabilities. For the sake of simplicity, we will find the explicit expressions at zero-gap  $\mu l_B = 0$ . One can notice that, at

the Dirac points  $\epsilon l_B = v_2 l_B$ , the GH shifts change their sign and behave differently. This change in sign of the GH shifts show clearly that they are strongly dependent on the barrier heights. We also observe that the GH shifts are negative and positive in Figures 2 and 3. Recall that, the Dirac points represent the zero modes for Dirac operator [21] and lead to the emergence of new Dirac points, which have been discussed in different works [36, 37]. Such points separate the two regions of positive and negative refraction. In the cases of  $\epsilon l_B < v_2 l_B$  and  $\epsilon l_B > v_2 l_B$ , the shifts are, respectively, in the forward and backward directions, due to the fact that the signs of group velocity are opposite. It is clearly seen that  $S_t$  are oscillating between negative and positive values around the critical point  $\epsilon l_B = v_2 l_B$ , in the interval when  $\epsilon l_B < v_1 l_B$  the usual high energy barrier oscillations appear either in Figure 2 or Figure 3.

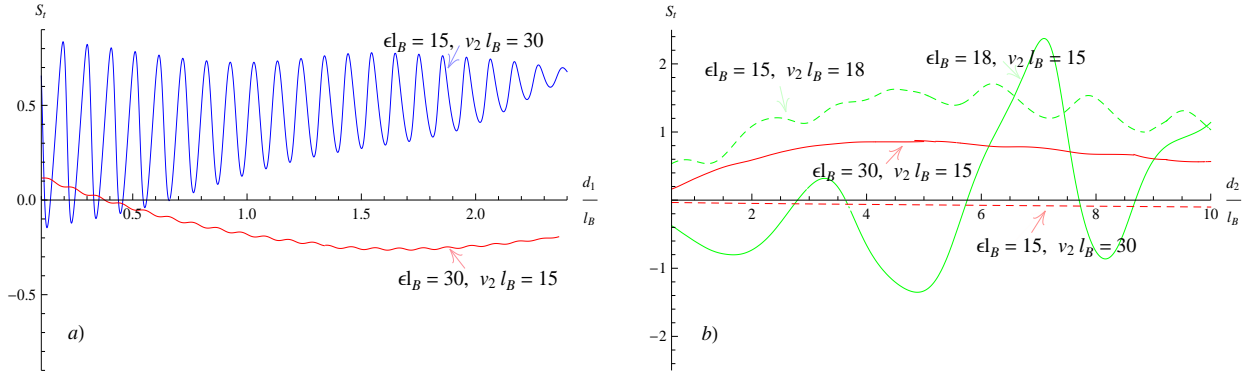


Figure 4: (Color online) The GH shifts in transmission  $S_t$  versus width  $\frac{d_1}{l_B}$  a) and width  $\frac{d_2}{l_B}$  b) for triangular double barrier. a): For  $\mu l_B = 0$ ,  $\frac{d_2}{l_B} = 2.5$ ,  $k_y l_B = 1$ ,  $v_1 l_B = 25$ ,  $(\epsilon = 15, v_2 = 30)$ ,  $(\epsilon = 30, v_2 = 15)$ . b): For  $\mu l_B = 0$ ,  $\frac{d_1}{l_B} = 0.5$ ,  $k_y l_B = 1$ ,  $v_1 l_B = 25$ ,  $(\epsilon l_B = 15, v_2 l_B = 18)$ ,  $(\epsilon l_B = 18, v_2 l_B = 15)$ ,  $(\epsilon l_B = 15, v_2 l_B = 30)$ ,  $(\epsilon l_B = 30, v_2 l_B = 15)$ .

We further explore the effects of the triangular double barrier widths  $d_1$  and  $d_2$  on the GH shifts in Figure 4 for both cases  $\epsilon l_B < v_2 l_B$  and  $\epsilon l_B > v_2 l_B$ . Figure 4a) shows an interesting behavior of the GH shifts in terms of the barrier width  $d_1$  where oscillations with different amplitudes appeared for the configuration  $(\epsilon l_B = 15, v_2 l_B = 30)$ . However such behavior completely changes when we reverse the choice of parameters, i.e.  $\{\epsilon l_B = 30, v_2 l_B = 15\}$  then  $S_t$  crosses from positive to negative behaviors. As far as the second barrier width  $d_2$  is concerned, from Figure 4b) we observe different oscillations by considering some values of the couple  $(\epsilon l_B, v_2 l_B)$ .

At this level, we turn to the discuss the influence of the induced gap  $\mu l_B$  in our system in the presence of a triangular double barrier and a magnetic field. Note that, the gap is introduced as shown in Figure 1 and therefore it affects the system energy according to the solution of the energy spectrum obtained in region 3. Figure 5 shows that the GH shifts in the propagating case can be enhanced by a gap opening at the Dirac point. This has been performed by fixing the parameters  $\frac{d_1}{l_B} = 1.1$ ,  $\frac{d_2}{l_B} = 1.5$ ,  $v_1 l_B = 25$ ,  $k_y l_B = 1$  and making different choices for the energy  $\epsilon l_B$  and potential  $v_2 l_B$ . Figure 5a) presents the GH shift in transmission  $S_t$  and transmission probability as a function of energy gap  $\mu l_B$ . For the configuration  $(\epsilon l_B = 15, v_2 l_B = 23)$  it is clear that one can still have positive shifts (blue line) and for the configuration  $(\epsilon l_B = 23, v_2 l_B = 15)$  the GH shifts are negative (red line). Note that for certain energy gap  $\mu l_B$ , there is no transmission possible and therefore the

GH shifts in transmission  $S_t$  vanish. As shown in Figure 5b), we plot the GH shifts in reflection  $S_r$  and the reflection probability as a function of energy gap  $\mu l_B$  and found that the GH shifts display sharp peaks inside the transmission gap. It is clearly seen that the GH shifts can be enhanced by a certain gap opening. Indeed, by increasing the gap we observe that the gap of transmission becomes broader, changing the transmission resonances and the modulation of the GH shifts. Note that for certain energy gap  $\mu l_B$ , there is total reflection and therefore the GH shifts in reflection  $S_r$  does not vanish. In fact, under the condition  $\mu l_B > |\epsilon l_B - v_2 l_B|$  every incoming wave is reflected. In summary it is shown that  $(S_r, R)$  on one hand and  $(S_t, T)$  on the other hand are very much related in their structure. Physically  $S_t$  is detected in the transmission region by placing a detector in the outgoing region and far away from the incident region. On the contrary  $S_r$  is detected by placing a detector in the incident region far way from the transmission region.

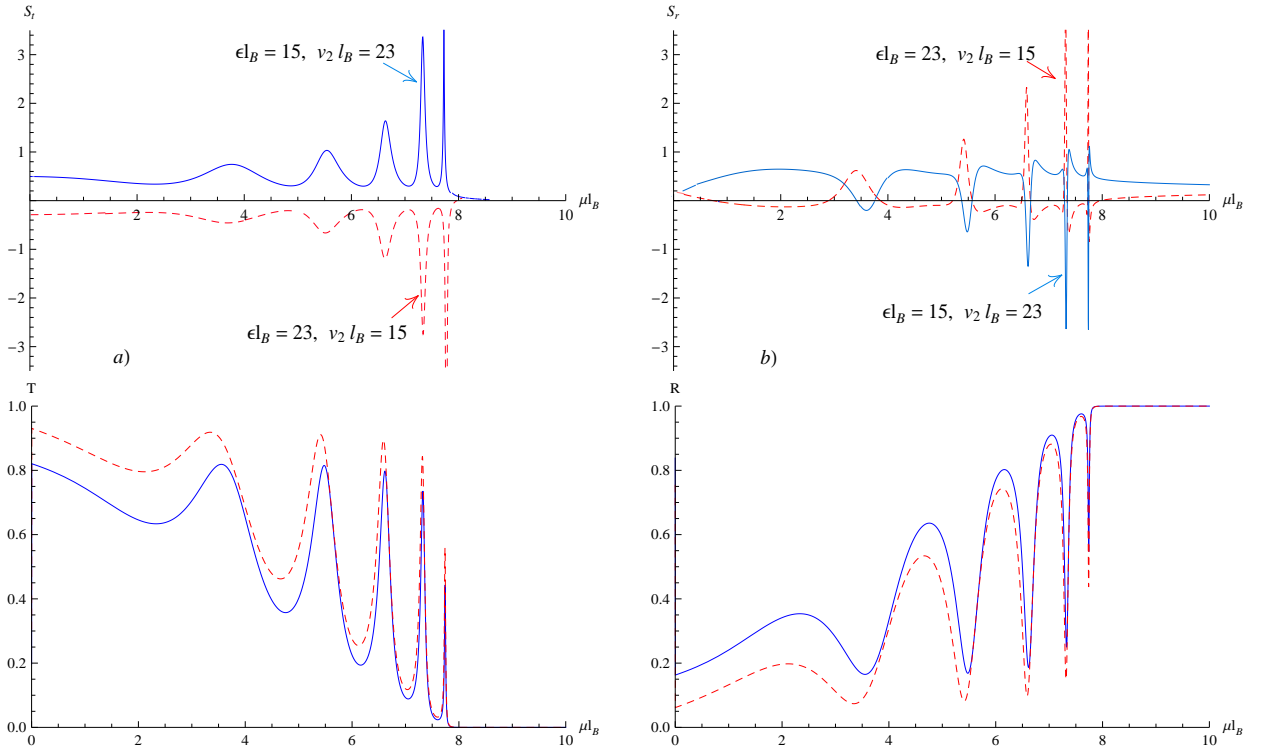


Figure 5: (Color online) a)/b): The GH shifts  $S_t/S_r$  and the probabilities  $T/R$  versus the energy gap  $\mu l_B$  with  $\frac{d_1}{l_B} = 1.1$ ,  $\frac{d_2}{l_B} = 1.5$ ,  $k_y l_B = 1$ ,  $v_1 l_B = 25$ ,  $(v_2 l_B = 23, \epsilon l_B = 15)$ ,  $(v_2 l_B = 15, \epsilon l_B = 23)$ .

Now let us investigate how the GH shifts behave as function of the barrier potential height  $v_2 l_B$  which shown numerically in Figure 6a) for different choices of the barriers width  $\frac{d_1}{l_B} = \{1.1, 0.5, 0.2\}$  and in Figure 6b) for different values of the energy gap  $\mu l_B = \{0, 2, 4\}$ . It is clearly seen that the GH shifts change their sign near the point  $v_2 l_B = \epsilon l_B$ . We notice that when the condition  $v_2 l_B > \epsilon l_B$  is fulfilled, the GH shifts are positive, while it becomes negative when the height of the barrier satisfies the condition  $v_2 l_B < \epsilon l_B$ . We observe from Figures 6a) and 6b) that the GH shifts are strongly dependent on the barrier height  $v_2 l_B$ , which can be experimentally implemented by applying a local top gate voltage  $v_2 l_B$  to graphene [29]. This tells us that the GH shifts can be controlled by changing the potential height  $v_2 l_B$ .

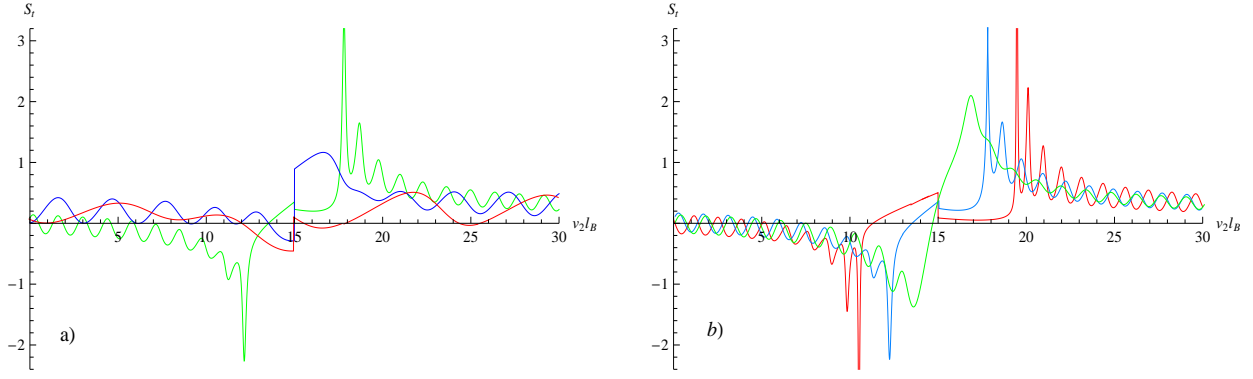


Figure 6: (Color online) The GH shifts  $S_t$  versus the second potential height  $v_2 l_B$  with  $\frac{d_2}{l_B} = 1.5$ ,  $k_y l_B = 1$ ,  $v_1 l_B = 25$ ,  $\epsilon l_B = 15$ . a):  $\mu l_B = 2$  and three different values of the barrier width  $\frac{d_1}{l_B} = 1.1$  green color,  $\frac{d_1}{l_B} = 0.5$  blue color,  $\frac{d_1}{l_B} = 0.2$  red color. b):  $\frac{d_1}{l_B} = 1.1$  and three different values of the gap  $\mu l_B = 0$  green color,  $\mu l_B = 2$  blue color,  $\mu l_B = 4$  red color.

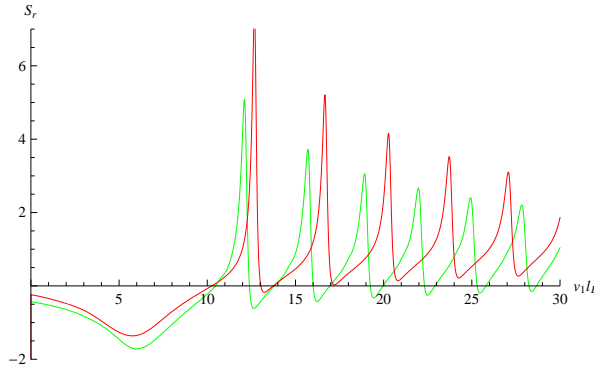


Figure 7: (Color online) The GH shifts  $S_r$  versus the first potential height  $v_1 l_B$  with  $\frac{d_2}{l_B} = 0.2$  green color,  $\frac{d_1}{l_B} = 0.5$  red color,  $\frac{d_2}{l_B} = 2.5$ ,  $k_y l_B = 1$ ,  $v_2 l_B = 10$ ,  $\epsilon l_B = 7$ ,  $\mu l_B = 4$ .

Figure 7 shows the GH shifts in reflection  $S_r$  through a graphene triangular double barriers with  $\frac{d_2}{l_B} = 2.5$ ,  $k_y l_B = 1$ ,  $v_2 l_B = 10$ ,  $\epsilon l_B = 7$ ,  $\mu l_B = 4$  and different values of the barrier width  $\frac{d_1}{l_B} = \{0.2, 0.5\}$ . The GH shifts  $S_r$  can be either negative or positive and can also be modulated for potential barrier  $v_1 l_B > v_2 l_B$ .

Figure 8 illustrates the dependence of the GH shift and transmission probability on the magnetic field  $B$ . For this, we choose three values  $B = 0.2T$  red color,  $B = 1.5T$  green color,  $B = 3T$  blue color and the other physical parameters are, respectively,  $\mu = 2$ ,  $d_1 = 1.1$ ,  $d_2 = 1.5$ ,  $k_y = 1$ ,  $v_1 = 25$ . As shown in Figure 8a), we plot the GH shifts in transmission  $S_t$  and the transmission probability  $T$  as a function of energy  $\epsilon$  with  $v_2 = 15$  and found that the GH shifts display sharp peaks inside the transmission gap. The GH shifts can be changed from positive to negative by controlling the strength of the magnetic field. However, the GH shifts finally become negative with increasing the strength of the magnetic fields. We can see that the transmission decreased with the increased magnetic fields. In Figure 8b) we plot the GH shifts in transmission  $S_t$  and the transmission probability  $T$  as a function of  $v_2$  with  $\epsilon = 15$ . The GH shifts change sign at the Dirac point  $v_2 = \epsilon$ . In particular the GH shifts in transmission can be negative and positive also the transmission probability decreased with

the increased magnetic fields.

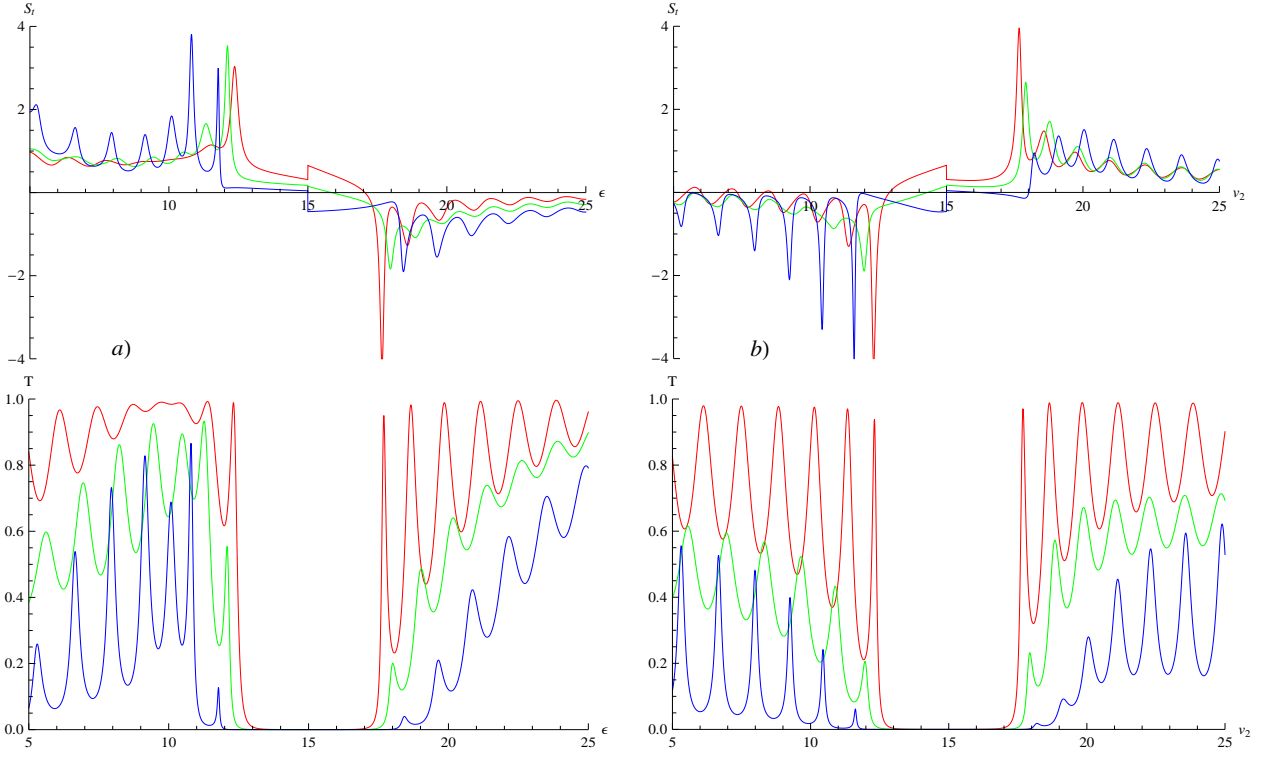


Figure 8: (Color online) a)/b) The GH shifts  $S_t$  and the probability transmission  $T$  b) versus the energy  $\epsilon/v_2$  for three different values of the magnetic field  $B = 0.2T$  red color,  $B = 1.5T$  green color,  $B = 3T$  blue color, with  $\mu = 2$ ,  $d_1 = 1.1$ ,  $d_2 = 1.5$ ,  $k_y = 1$ ,  $v_1 = 25$ ,  $v_2 = 15/\epsilon = 15$ .

## 6 Conclusion

We have investigated the Goos-Hänchen (GH) shifts for Dirac fermions in graphene scattered by triangular double barriers and in the presence of a uniform magnetic field. In the first stage, we have solved the eigenvalue equation to end up with the solutions of the energy spectrum in terms of different physical parameters characterizing the five regions composing the present system.

In the second stage, we have used the continuity conditions at each interface of the five regions and used the transfer matrix method to explicitly determine the transmission and reflection coefficients. To make a link with optics system, we have mapped our eigenspinor solutions as the incident, reflected and transmitted beams together with a Gaussian function. Subsequently, we have written the obtained coefficients in complex notation to get the transmission and reflection angles. These were used together with the transverse wave vector  $k_y$  around a point  $k_{y0}$  to derive the corresponding GH shifts in transmission and in reflection amplitudes.

Different numerical results were presented in terms of the physical parameters characterizing the present system. In fact, Our results show that the GH shifts are affected by the internal structure of the triangular double barriers. In particular, the GH shifts change sign at the transmission zero energies and peaks at each bound state associated with the triangular double barriers. It is observed

that the GH shifts can be enhanced by the presence of resonant energies in the system when the incident angle is less than the critical angle associated with total reflection.

## Acknowledgments

The generous support provided by the Saudi Center for Theoretical Physics (SCTP) is highly appreciated by all authors. AJ and HB acknowledge the support of King Fahd University of Petroleum and minerals under research group project RG171007.

## References

- [1] Quantum-Classical Analogies, edited by D. Dragoman, M. Dragoman (Springer, Berlin, 2004)
- [2] F. Goos and H. Hänchen, Ann. Phys. 1, 333 (1947); *ibid* 5, 251 (1949).
- [3] T. K. Gaylord, E. N. Glytsis, G. N. Henderson, K. P. Martin, D. B. Walker, D. W. Wilson, K. F. Brennan, Proc. IEEE 79, 1159 (1991)
- [4] P. Wallace, Phys. Rev. 71, 622 (1947).
- [5] K. S. Novoselov, A. K. Geim, S. V. Morozov, D. Jiang, Y. Zhang, S. V. Dubonos, I. V. Grigorieva and A. A. Firsov, Science 306, 666 (2004).
- [6] N. Stander, B. Huard and D. Goldhaber-Gordon, Phys. Rev. Lett. 102, 026807 (2009).
- [7] M. I. Katsnelson, K. S. Novoselov and A. K. Geim, Nature Phys. 2, 620 (2006).
- [8] H. Sevincli, M. Topsakal and S. Ciraci, Phys. Rev. B 78, 245402 (2008).
- [9] M. R. Masir, P. Vasilopoulos and F. M. Peeters, New J. Phys. 11, 095009 (2009).
- [10] L. Dell’Anna and A. De Martino, Phys. Rev. B 79, 045420 (2009).
- [11] S. Mukhopadhyay, R. Biswas and C. Sinha, Phys. Status Solidi B 247, 342 (2010).
- [12] E. B. Choubabi, M. El Bouziani and A. Jellal, Int. J. Geom. Meth. Mod. Phys. 7, 909 (2010).
- [13] H. Bahlouli, E. B. Choubabi, A. Jellal and M. Mekkaoui, J. Low Temp. Phys. 169, 51 (2012).
- [14] A. Jellal and A. El Mouhafid, J. Phys. A: Math. Theo. 44, 015302 (2011).
- [15] J. Tworzydło, B. Trauzettel, M. Titov, A. Rycerz and C. W. J. Beenakker, Phys. Rev. Lett. 96, 246802 (2006).
- [16] H. Bahlouli, E.B. Choubabi, A. EL Mouhafid and A. Jellal, Solid State Communications 151 (2011) 1309.
- [17] K. Artmann, Ann. Physik 2, 87 (1949)
- [18] X. Chen, J.-W. Tao, and Y. Ban, Eur. Phys. J. B 79, 203 (2011).

- [19] Y. Song, H-C. Wu and Y. Guo, Appl. Phys. Lett. 100, 253116 (2012).
- [20] X. Chen, P-L. Zhao, X-J. Lu and L-G. Wang, Eur. Phys. J. B 86, 223 (2013).
- [21] M. Sharma and S. J. Ghosh, Phys.: Condens. Matter 23, 055501 (2011).
- [22] J.-H. Huang, Z.-L. Duan, H.-Y. Ling, and W.-P. Zhang, Phys. Rev. A 77, 063608 (2008).
- [23] C. W. J. Beenakker, R. A. Sepkhanov, A. R. Akhmerov and J. Tworzydło, Phys. Rev. Lett. 102, 146804 (2009).
- [24] L. Zhao and S. F. Yelin, Phys. Rev. B 81, 115441 (2010).
- [25] L. Jiang, J. Wu, X. Dai, and Y. Xiang, Optik 125, 7025 (2014).
- [26] L. Jiang, Q. Wang, Y. Xiang, X. Dai, and S. Wen, IEEE Photonics J. 5, (2013).
- [27] Q. You, L. Jiang, X. Dai, and Y. Xiang, Chinese Phys. B 27, 094211 (2018).
- [28] Q. You, Y. Shan, S. Gan, Y. Zhao, X. Dai, and Y. Xiang, Opt. Mater. Express 8, 3036 (2018).
- [29] M. Mekkaoui, A. Jellal and H. Bahlouli, Physica E 87, 266 (2017).
- [30] E. Sonin, Phys. Rev. B 79, 195438 (2009).
- [31] M. Abramowitz and I. Stegun, Handbook of Integrals, Series and Products, (Dover, New York, 1956).
- [32] L. Gonzalez-Diaz and V. M. Villalba, Phys. Lett. A 352, 2 02 (2006).
- [33] D. Bohm, Quantum Theory, (Prentice-Hall, New York, 1951), pp. 257-261.
- [34] A. Jellal, I. Redouani, Y. Zahidi and H. Bahlouli, Physica E 58, 30 (2014).
- [35] A. Jellal, Y. Wang, Y. Zahidi and M. Mekkaoui, Physica E 68, 53 (2015).
- [36] S. Bhattacharjee, M. Maiti and K. Sengupta, Phys. Rev. B 76, 184514 (2007).
- [37] C. H. Park, L. Yang, Y. W. Son, M. L. Cohen and S. G. Louie, Phys. Rev. Lett. 101, 126804 (2008).